British Journal of Pharmacology

British Journal of Pharmacology (2017) **174** 2409–2421 2409

RESEARCH PAPER

Design and validation of the first cell-impermeant melatonin receptor agonist

Correspondence Ralf Jockers, Institut Cochin, 22 Rue Méchain, 75014 Paris, France. E-mail: ralf.jockers@inserm.fr

Received 9 March 2017; **Revised** 27 April 2017; **Accepted** 3 May 2017

Florence Gbahou[1,2,3,*], Erika Cecon[1,2,3,*], Guillaume Viault[4], Romain Gerbier[1,2,3], Frederic Jean-Alphonse[5], Angeliki Karamitri[1,2,3], Gérald Guillaumet[4], Philippe Delagrange[6], Robert M Friedlander[7], Jean-Pierre Vilardaga[5], Franck Suzenet[4] and Ralf Jockers[1,2,3]

[1]Inserm, U1016, Institut Cochin, Paris, France, [2]CNRS UMR 8104, Paris, France, [3]Université Paris Descartes, Paris, France, [4]Institut de Chimie Organique et Analytique (ICOA), Université d'Orléans, UMR CNRS 7311, B.P. 6759, Orléans Cedex 2, France, [5]Laboratory for GPCR Biology, Department of Pharmacology and Chemical Biology, University of Pittsburgh School of Medicine, Pittsburgh, PA, USA, [6]Pôle d'Innovation Thérapeutique Neuropsychiatrie, Institut de Recherches Servier, Croissy, France, and [7]Neuroapoptosis Laboratory, Department of Neurological Surgery, University of Pittsburgh, Pittsburgh, PA, USA

*These authors contributed equally.

BACKGROUND AND PURPOSE

The paradigm that GPCRs are able to prolong or initiate cellular signalling through intracellular receptors recently emerged. Melatonin binds to G protein-coupled MT_1 and MT_2 receptors. In contrast to most other hormones targeting GPCRs, melatonin and its synthetic analogues are amphiphilic molecules easily penetrating into cells, but the existence of intracellular receptors is still unclear mainly due to a lack of appropriate tools.

EXPERIMENTAL APPROACH

We therefore designed and synthesized a series of hydrophilic melatonin receptor ligands coupled to the Cy3 cyanin fluorophore to reliably monitor its inability to penetrate cells. Two compounds, one lipophilic and one hydrophilic, were then functionally characterized in terms of their affinity for human and murine melatonin receptors expressed in HEK293 cells and their signalling efficacy.

KEY RESULTS

Among the different ligands, ICOA-13 showed the desired properties as it was cell-impermeant and bound to human and mouse MT_1 and MT_2 receptors. ICOA-13 showed differential activities on melatonin receptors ranging from partial to full agonistic properties for the G_i/cAMP and ERK pathway and β-arrestin 2 recruitment. Notably, ICOA-13 enabled us to discriminate between G_i/cAMP signalling of the MT_1 receptor initiated at the cell surface and neuronal mitochondria.

CONCLUSIONS AND IMPLICATIONS

We report here the first cell-impermeant melatonin receptor agonist, ICOA-13, which allows us to discriminate between signalling events initiated at the cell surface and intracellular compartments. Detection of mitochondrial MT_1 receptors may have an important impact on the development of novel melatonin receptor ligands relevant for neurodegenerative diseases, such as Huntington disease.

Abbreviations

2-[^{125}I]-MLT, 2-[^{125}I]-iodomelatonin; Fsk, forskolin

DOI:10.1111/bph.13856

Introduction

Melatonin, N-acetyl-5-methoxytryptamin, is derived from 5-HT (serotonin) in a two-step biosynthetic pathway that exists in most organisms. In mammals, melatonin is primarily produced by the pineal gland in a circadian manner with high levels during the night. Due to its lipophilic property, melatonin rapidly distributes all over the brain and in peripheral tissues (Reiter *et al.*, 2014) playing an important role on the synchronization of physiological rhythms and on the regulation of various neuronal, retinal, immunological and metabolic functions (Dubocovich *et al.*, 2010; Tosini *et al.*, 2014). Most effects of melatonin are mediated by melatonin **MT_1** and **MT_2** receptors belonging to the large family of GPCRs. Both melatonin receptors are preferentially coupling to proteins of the $G_{i/o}$ sub-family (Jockers *et al.*, 2016).

The lipophilic characteristic of melatonin raised since its discovery the intriguing possibility that this neurohormone might bind to molecular targets located not only at the cell surface but also in intracellular compartments. Several putative intracellular melatonin binding proteins have been reported such as calmodulin, the enzyme quinone reductase 2 (Jockers *et al.*, 2008) and RORα/RZR nuclear receptors (Becker-Andre *et al.*, 1994). However, the interaction between melatonin and most of these targets remains highly controversial (Jetten, 2009). In addition, increasing evidence indicates that GPCRs are able to signal through heterotrimeric G proteins not only at the plasma membrane but also in intracellular compartments (Vilardaga *et al.*, 2014; Irannejad *et al.*, 2015). Recent evidence suggests that the MT_1 receptor has mitochondrial functions in neurons that might be mediated by intracellular receptors (Zhang *et al.*, 2013) and that are altered in Huntington disease (Wang *et al.*, 2011). Moreover, significant levels of endogenous melatonin have been measured in brain mitochondria (Venegas *et al.*, 2012), raising the possibility of an autocrine action. A significant amount of data evidencing melatonin-dependent regulation of mitochondria function supports this scenario (reviewed by Tan *et al.*, 2016). Reduced melatonin production is commonly observed in neurodegenerative diseases, including Huntington and Alzheimer's disease (Liu *et al.*, 1999; Kalliolia *et al.*, 2014), which launched the therapeutic use of melatonin and its analogues in several pathologies. However, only modest beneficial effects are usually reported, pointing to the need of a better understanding of the mechanism of action underlying the effects of melatonin. To better distinguish between cell surface and intracellular melatonin targets, we designed a series of melatonin derivatives coupled to the hydrophilic Cy3 cyanin fluorophore with the goal to generate a hydrophilic melatonin receptor ligand that would not penetrate into cells.

Methods

HEK293 cell culture

HEK293 cells were grown in complete DMEM medium, supplemented with 10% ($v \cdot v^{-1}$) FBS, 4.5 $g \cdot L^{-1}$ glucose, 100 $U \cdot mL^{-1}$ penicillin and 0.1 $mg \cdot mL^{-1}$ streptomycin and maintained at 37°C (95% O_2, 5% CO_2). Transient transfection of cells was performed with the JetPEI reagent according to the supplier's instructions (Polyplus-transfection, New York, NY, USA).

Radioligand binding experiments

Membranes from HEK293 cells transiently expressing human or murine MT_1 or MT_2 receptors were prepared as previously described (Ayoub *et al.*, 2004). **2-[^{125}I]-iodomelatonin** (2-[^{125}I]-MLT) saturation binding experiments were performed in the range of 1–1000 pM, and specific binding was defined as binding displaced by 10 μM iodomelatonin. Competition curves were performed by simultaneous incubation of 2-[^{125}I]-MLT (100 pM) and increasing concentrations of the respective ligands. Assays were carried out in duplicates for 120 min at 37°C, followed by rapid filtration through GF/F glass fibre filters (Whatman, Clifton, NJ, USA). Filter-retained radioactivity was determined with a γ-counter LB2111 (Berthold Technologies, Bad Wildbad, Germany). K_i values were calculated from IC_{50} values using the Cheng–Prussof formula: $K_i = IC_{50}/[1 + (L/K_d)]$ where L represents the ligand concentration and K_d the dissociation constant. K_d values were 148 ± 8; 397 ± 30; 330 ± 128; and 95 ± 20 pM (n = 3) for hMT_1, hMT_2, mMT_1 and mMT_2 receptors respectively.

Fluorescence microscopy

Non-transfected HEK293 cells (10^5 cells per well) were plated on 4-well chamber-slide plates (Nunc® Lab-Tek®, Sigma-Aldrich) and maintained at 37°C, 5% CO_2 overnight. Cells were washed in PBS, fixed in 4% paraformaldehyde (15 min, −20°C), followed by treatment with TritonX-100 (0.2%, 1 h) in order to permeabilize the cells, while another group of wells were kept intact. Cells were incubated in the presence of the fluorescent compounds ICOA-9 or ICOA-13 (100 nM, 4 h), washed with PBS and incubated with DAPI (1:2000 dilution, 5 min; Santa Cruz Biotechnology, Dallas, TX, USA) to stain the cell nuclei. The slides were mounted and analysed by fluorescence microscopy. Images were acquired under 63× oil objective using specific excitation/emission filters to image ICOA-9 (ex/em 508/516 nm), or ICOA-13 (ex/em 565/580 nm) and DAPI (ex/em 358/461 nm). Images were analysed using ImageJ software (National Institutes of Health, USA).

ERK1/2 activation assays

Total ERK and phospho-ERK1/2 was detected by SDS-PAGE/immunoblot analysis, as previously described (Cecon *et al.*, 2015). Briefly, HEK293 cells transfected to express mMT_1, mMT_2, hMT_1 or hMT_2 receptors were starved (overnight) before addition of the ligands melatonin (100 nM), ICOA-9 (1 μM) or ICOA-13 (1 μM) for 5 min (37°C 5% CO_2). Pertussis toxin treatment (10 $ng \cdot \mu L^{-1}$) was performed during the starvation. After the incubation, cells were washed in PBS, harvested in lysis buffer, and denaturated proteins were resolved in 12% SDS-PAGE gels. Following the transfer of proteins to nitrocellulose membranes, the membranes were immunoblotted with antibodies against ERK (1:3000 dilution, sc-154, Santa Cruz Biotechnology) and phospho-ERK1/2 (1:1000 dilution, sc-7383; Santa Cruz Biotechnology) and developed using appropriate secondary antibodies.

Membranes were analysed using the Odyssey LI-COR infrared fluorescent scanner (LI-COR Biosciences, Lincoln, NE, USA).

For quantitative analysis of ERK activation, we used the P-ERK AlphaScreen SureFire Assay kit (TGR BioSciences, Adelaide, Australia; and PerkinElmer, Waltham, MA, USA). Cells were stimulated as described above, collected in lysis buffer, and 4 μL of each sample was used for the assay, following the supplier's instructions. The plate was read using the Infinite M1000 Tecan microplate reader. No effect was observed in non-transfected HEK293 cells up to 10 μM of the two fluorescent compounds (ICOA-9, ICOA-13). Data were fitted by non-linear regression to determine E_{max} and EC_{50} values and normalized to the basal levels using GraphPad Prism software (La Jolla, CA, USA).

Accumulative cAMP assay

The cAMP assay was performed as previously described (Kamal *et al.*, 2015). Briefly, HEK293 cells expressing mMT_1, mMT_2, hMT_1 or hMT_2 receptors were dispensed into a 384-well plate (4000 cells per well) and stimulated with 2 μM forskolin in the presence of increasing concentrations of melatonin, ICOA-9 or ICOA-13 for 30 min at room temperature in PBS buffer supplemented with 1 mM IBMX (Sigma-Aldrich, St Quentin, France). Cells were then lysed, and cAMP levels were determined following the manufacturer's instruction (Cisbio Bioassays, Codolet, France). The plate was read using the Infinite F500 Tecan microplate reader. No effect was observed in non-transfected HEK293 cells up to 10 μM of ICOA-9 and 1 μM of ICOA-13. Data were fitted by non-linear regression to determine E_{max} and EC_{50} values and normalized to forskolin-induced response (100%) and melatonin-induced maximum inhibition (0%) using GraphPad Prism software.

Time-course measurements of cAMP production

cAMP was assessed in live neuroblastoma N2a cells using a fluorescent resonance energy transfer (FRET)-based assay. cAMP levels were measured either at the plasma membrane or at the outer mitochondrial membrane by transfecting the cells with FRET-based biosensors (DiPilato *et al.*, 2004; Feinstein *et al.*, 2013). Cells plated on poly-D-lysine-coated glass were mounted in Attofluor cell chambers and transferred on the Nikon Ti-E confocal microscope. Cyan Fluorescent Protein (CFP) and Yellow Fluorescent Protein (YFP) were excited using a mercury lamp, and the emissions (filters: 480 ± 20 nm for CFP and 535 ± 15 nm for YFP) were simultaneously detected with a LUCAS EMCCD camera (Andor Technology). Fluorescence data were extracted from single cells using Nikon Element Software (Nikon Corporation, Minato-ku, Tokio, Japan), as previously described (Ferrandon *et al.*, 2009). Data were normalized to the forskolin-induced response. Cells were continuously perfused with buffer or with the corresponding ligand for the indicated time.

ß-arrestin2 recruitment assay

The PathHunter™ assay from the DiscoverX company was used to measure the recruitment of β-arrestin2 to melatonin receptors (DiscoverX, Birmingham, United Kingdom). Briefly, HEK293 parental cells stably expressing a fusion protein of β-arrestin2 and the larger N-terminal deletion mutant of β-gal were transiently transfected with hMT_1 or hMT_2 receptors fused at their C-terminal part with the small enzyme fragment ProLink tag. Two days after transfection, the cells were treated with increasing concentrations of melatonin, ICOA-9 or ICOA-13 for 2–3 h at 37°C. β-arrestin2 recruitment resulted in the complementation of the two enzyme fragments and the formation of an active β-gal enzyme. Luminescence signals were determined after 60 min incubation at room temperature. No effect was observed in parental HEK293/ß-arrestin2 cells in the absence of melatonin receptors up to 10 μM of ICOA-9 and 1 μM of ICOA-13. Data were fitted by non-linear regression to determine E_{max} and EC_{50} values and normalized to basal levels (0%) and to maximum melatonin-induced response (100%) using GraphPad Prism software.

Bias calculation

The dose–response curves were fitted to the operational model of agonism designed by Kenakin and Christopoulos (Kenakin and Christopoulos, 2013; Kenakin *et al.*, 2012) to obtain $\log(\tau/K_A)$ transduction ratios that are a unique index of coupling efficiency (or efficacy) of the agonist. To eliminate the influence of the system and the observation biases, the activity of the compounds at a given signalling pathway was compared with that of melatonin which served as the reference compound, and subsequently, values are expressed as $\Delta\log(\tau/K_A)$. The bias between two ligands is expressed as $10^{\Delta\Delta\log(\tau/KA)}$ as described previously (van der Westhuizen *et al.*, 2014). The significance of the ligand biases was determined by Student's two-tailed unpaired *t*-test. Because we did not reach a plateau for the two fluorescent compounds for ERK activation, we used the extrapolated data for EC_{50} and E_{max} as derived from GraphPad Prism using a non-linear regression analysis to obtain an estimate of the bias factor at hMT_1 receptors, following the same procedure as previously applied by the Christopoulos lab (Baltos *et al.*, 2016). The estimated pEC_{50} values were −6.35 ± 0.52 (E_{max} = 112 ± 6) and −5.60 ± 0.32 (E_{max} = 128 ± 15) for ICOA-9 and ICOA-13 respectively.

Data and statistical analysis

The data and statistical analysis comply with the recommendations on experimental design and analysis in pharmacology (Curtis *et al.*, 2015). Data are presented as means ± SEM of *n* independent experiments, performed at least in duplicates to ensure the reliability of single values. EC_{50} and E_{max} values were obtained following non-linear regression (curve fit) with four parameters of data from a minimum of eight different concentrations per experiment, repeated at least three times independently. All assays performed in this study were previously validated and demonstrated the robustness and variability of the procedure using this number of independent experiments for concentration–response curves. Statistical analysis was performed by Student's *t*-test when comparing only two groups. Values of $P < 0.05$ were considered statistically significant. When possible, data were normalized to maximal and minimum responses using melatonin response as a reference in order to avoid unwanted sources of variations, as differences in the amplitude of melatonin effect between independent experiments. Data and statistical analysis were performed using GraphPad Prism software version 6.

Materials

Melatonin and iodomelatonin were purchased from Sigma-Aldrich (St. Louis, MO, USA) and 2-[^{125}I]-MLT from PerkinElmer (Waltham, MA, USA).

cDNA constructs

Expression vectors for Flag-hMT$_1$, hMT2, Flag-mMT$_1$ and 6Myc-mMT$_2$, hMT$_1$-GFP have been validated and described previously (Petit *et al.*, 1999; Guillaume *et al.*, 2008; Baba *et al.*, 2013). Expression vectors for 3Myc-MT$_2$-PK2 and Flag-MT$_1$-PK2 were obtained from DiscoverX Corporation Ltd (Birmingham, UK).

Organic synthesis

All reagents were purchased from the commercial suppliers Sigma-Aldrich (St. Louis, MO, USA) and Alfa Easer (Karlsruhe, Germany) and were used without further purification.

Tetrahydrofuran was purified with a dry station GT S100, dichloromethane was distillated over calcium hydridre, triethylamine and diisopropylethylamine and dimethylformamide were distillated over CaH_2. The reactions were monitored by TLC analysis using silica gel (60 F254) plates. Compounds were visualized by UV irradiation and/or spraying with a solution of cerium molybdate, or phosphomolubdic acid, followed by heating at 200°C. Flash column chromatography was performed on silica gel 60 (230–400 mesh, 0.040–0.063 mm). Reversed-phase column flash-chromatographies were performed on octadecyl-functionalized silica gel (mean pore size 60 Å) from Aldrich. Cy 3.29 was synthesized according to reported literature procedure (Mujumdar *et al.*, 1993). ^{1}H and ^{13}C NMR spectra were recorded on a spectrometer at 250 MHz (^{13}C, 62.9 MHz) or 400 MHz (^{13}C, 100 MHz). The ^{1}H and ^{13}C NMR spectra for compounds 2, 5 and 7 (ICOA-13) are provided in Supplementary Information Figures S7–S9. Chemical shifts are given in parts per million from tetramethylsilane as internal standard. The following abbreviations are used for the proton spectra multiplicities: s, singulet; d, doublet; t, triplet; q, quartet; qt, quintuplet; m, multiplet; br, broad. Coupling constants (*J*) are reported in Hertz (Hz). Signals were assigned as far as possible by means of two-dimensional NMR spectroscopy: ^{1}H-^{1}H-COSY, ^{1}H-^{13}C-COSY (HSQC, heteronuclear single quantum coherence).

Ionspray methodology was used to record mass spectra. High Resolution Mass Spectrometry (HRMS) spectra were recorded on a Maxis Bruker 4G. The infrared spectra of compounds were recorded on a Thermo Scientific Nicolet iS10. Melting points [mp (°C)] were taken on open capillary tubes and are uncorrected, performed on a Electrothermal IA 9100.

(E)-1-(6-(4-(3-(2-acetamidoethyl)-5-methoxy-1H-pyrrolo[3,2-b]pyridin-2-yl)benzylamino)-6-oxohexyl)-2-((E)-3-(1-ethyl-3,3-dimethyl-5-sulfo-3H-indolium-2-yl)allylidene)-3,3-dimethylindoline-5-sulfonate (compound 2)

Under Argon, DIEA (25.0 µL, 0.14 mmol, 3.00 eq.) was added to a solution of Cy3.29 (30.0 mg, 47.0 µmol, 1.00 eq.) and TSTU (14.0 mg, 48.0 µmol, 1.01 eq.) in dry DMF (1 mL). The resulting solution was protected from the light and stirred 2 h at room temperature. A solution of the amine **1** (47.0 mg, 0.14 mmol, 3.00eq.) dissolved in dry DMF (1.5 mL) was then added to the mixture which was stirred overnight at room temperature. After removing the DMF under reduced pressure, the residue was purified on C18 reverse-phase chromatography with a gradient (methanol/water from 25:75 to 4:6). The fractions containing the desired compound were lyophilized to provide the compound **2** as a pink solid (18.0 mg, 40% yield).

^{1}H NMR (400 MHz, MeOD): δ 8.54 (t, *J* = 13.4 Hz, 1H), 7.99–7.94 (m, 2H), 7.91 (d, *J* = 8.4 Hz, 2H), 7.79 (d, *J* = 8.7 Hz, 1H), 7.62 (d, *J* = 8.1 Hz, 2H), 7.38 (dd, *J* = 15.4, 8.4 Hz, 4H), 6.67 (d, *J* = 8.7 Hz, 1H), 6.51 (dd, *J* = 13.4, 10.1 Hz, 2H), 4.41 (s, 2H), 4.18 (dd, *J* = 7.1, 3.8 Hz, 4H), 4.02 (s, 3H), 3.50 (t, *J* = 7.3 Hz, 2H), 3.09 (t, *J* = 7.3 Hz, 2H), 2.32 (t, *J* = 7.1 Hz, 2H), 1.98–1.66 (m, 16H), 1.57–1.46 (m, 2H), 1.39 (t, *J* = 6.6 Hz, 3H).

^{13}C NMR (101 MHz, MeOD): δ 175.3, 175.1, 174.3, 171.8, 159.3, 151.4, 143.3, 142.8, 142.7, 142.6, 140.9, 140.8, 138.8, 131.4, 127.8, 127.7, 126.8, 125.4, 120.1, 120.1, 110.7, 110.5, 103.2, 103.1, 44.0, 42.4, 39.8, 39.2, 35.2, 26.8, 26.7, 25.9, 25.0, 23.3, 21.2, 17.3, 15.9, 11.2.

IR: ν_{max} (cm^{-1}) = 3273, 2930, 1645, 1553, 1433, 1415, 1173, 1109, 1064, 1019, 926, 686.

HRMS (ESI): m/z = 951.3779 [M + H]$^+$ calculated for $C_{50}H_{59}N_6O_9S_2$, found: m/z = 951.3764.

Melting point: 271°C.

(E)-2-((E)-3-(1-(6-((2-((3-(2-acetamidoethyl)-1H–pyrrolo[3,2-b]pyridin-5-yl)oxy)ethyl)amino)-6-oxohexyl)-3,3-dimethyl-5-sulfo-3H-indol-1-ium-2-yl)allylidene)-1-ethyl-3,3-dimethylindoline-5-sulfonate (compound 5)

Under Argon, DIEA (25.0 µL, 0.14 mmol, 3.00 eq.) was added to a solution of Cy3.29 (30.0 mg, 47.0 µmol, 1.00 eq.) and TSTU (14.0 mg, 48.0 µmol, 1.01 eq.) in dry DMF (1 mL). The resulting solution was protected from the light and stirred for 2 h at room temperature. A solution of the amine **4** (37.0 mg, 0.14 mmol, 3.00 eq.) dissolved in dry DMF (1.5 mL) was then added to the mixture which was stirred overnight at room temperature. After removing of the DMF under reduced pressure, the residue was purified on C18 reverse-phase chromatography with a gradient (methanol/water from 25:75 to 4:6). The fractions containing the desired compound were lyophilized to provide the compound **5** as a pink solid (22.0 mg, 53% yield).

^{1}H NMR (400 MHz, D_2O): δ 8.38 (t, *J* = 13.6 Hz, 1H, H19), 7.87 (s, 1H, H21), 7.83 (s, 1H, H21), 7.55 (d, *J* = 8.7 Hz, 1H, H7), 7.26 (d, *J* = 8.1 Hz, 1H), 7.21 (s, 1H), 7.17 (d, *J* = 8.5 Hz, 1H), 6.59 (d, *J* = 8.7 Hz, 1H, H6), 6.26 (d, *J* = 13.4 Hz, 1H, H20), 6.14 (d, *J* = 13.2 Hz, 1H, H18), 4.53–4.48 (m, 1H), 4.32 (t, *J* = 5.4 Hz, 1H, H11), 4.02 (d, *J* = 7.0 Hz, 2H, H17), 3.72 (d, *J* = 6.8 Hz, 2H, H24), 3.70–3.64 (m, 1H), 3.54 (t, *J* = 4 Hz, 2H, H12), 3.30 (t, *J* = 7.2 Hz, 2H, H8), 3.00–2.94 (m, 2H, H14), 2.75 (t, *J* = 7.2 Hz, 2H, H9), 2.27 (t, *J* = 6.4 Hz, 2H, H13), 1.86 (bs, 2H,), 1.65 (s, 6H, 2 x CH3), 1.60 (s, 6H, 2 x CH3), 1.31 (dd, *J* = 16.0, 8.6 Hz, 3H, H25), 1.26 (dd, *J* = 7.1, 6.0 Hz, 2H, H 15).

^{13}C NMR (101 MHz, MeOD): δ 175.41, 175.10, 174.67, 171.68, 158.63, 151.43, 143.11, 142.70, 142.68, 142.64,

141.33, 140.88, 140.76, 126.84, 125.34, 125.27, 121.98, 120.07, 111.71, 110.69, 110.47, 104.10, 103.22, 103.06, 63.73, 43.89, 40.00, 39.21, 38.85, 35.25, 26.84, 26.67, 26.62, 25.65, 24.96, 23.84, 21.32, 11.22.

HRMS (ESI): m/z = 873.3320 $[M-H]^-$ calculated for $C_{44}H_{53}N_6O_9S_2$, found: m/z = 873.3312.

IR: ν_{max} (cm^{-1}) = 3292, 2923, 2853, 1651, 1556, 1434, 1415, 1175, 1109, 1065, 1020, 927, 687.

Melting point: 186°C.

E-1-(6-(2-(3-(2-acetamidoethyl)-5-methoxy-1H-pyrrolo[3,2-b]pyridin-1-yl)ethylamino)-6-oxohexyl)-2-((E)-3-(1-ethyl-3,3-dimethyl-5-sulfo-3H-indolium-2-yl)allylidene)-3,3-dimethylindoline-5-sulfonate (compound 7)

Dry DIEA (16 μL, 12 mg, 95 μmol, 3 eq.) was added to a solution of Cy3.29 (20 mg, 32 μmol, 1 eq.) and TSTU (10 mg, 32 μmol, 1.01 eq.) in dry DMF (1 mL). The resulting solution was protected from the light and stirred 2 h at room temperature under an atmosphere of argon. Thereafter, a solution of the amine **6** (26 mg, 95 μmol, 3 eq.) in dry DMF 1 mL was added, and the mixture was stirred overnight at room temperature. After removing the DMF, the residue was purified by reversed flash chromatography with 25 to 40% of MeOH in ultra-pure water as eluent. The product-containing fractions were lyophilized to provide the compound **7** as a pink solid (25 mg, 89% yield).

^{1}H NMR (400 MHz, D_2O): δ = 8.35 (t, *J* = 13.5, 1H), 7.85 (m, 4H), 7.67 (d, *J* = 8.9 Hz, 1H), 7.26 (m, 3H), 6.49 (d, *J* = 8.9 Hz, 1H), 6.24 (d, *J* = 13.4 Hz, 2H), 4.07 (t, *J* = 6.2 Hz, 2H), 3.90 (m, 4H), 3.73 (s, 3H), 3.41 (t, *J* = 6.0 Hz, 2H), 3.21 (m, 4H), 2.71 (t, *J* = 7.0 Hz, 2H), 2.05 (t, *J* = 6.9 Hz, 2H), 1.85 (s, 3H), 1.65 (t, *J* = X Hz, 2H), 1.41 (m, 14 H), 1.21 (t, *J* = 7.2 Hz, 3H).

^{13}C NMR (101 MHz, D_2O): δ 176.1, 175.6, 175.0, 173.4, 159.4, 151.5, 143.7, 143.2, 141.3, 141.3, 141.0, 139.9, 139.8, 129.3, 126.7, 126.0, 121.4, 119.8, 119.7, 111.3, 111.2, 111.1, 103.1, 102.9, 53.9, 49.2, 49.1, 48.7, 44.8, 43.8, 39.9, 39.4, 35.3, 27.0, 26.7, 26.3, 25.1, 24.5, 23.1, 21.9, 20.0, 11.5.

IR: ν_{max} (cm^{-1}) = 928, 1022, 1111, 1186, 1435, 1555, 1648, 2935, 3294.

HRMS (ESI): m/z = 443.1712 $[M-2H]^{2-}$ calculated for $C_{45}H_{56}N_6O_9S_2$, found: m/z = 443.1697.

Melting point: 281°C.

Photophysical measurements

UV–visible spectra were obtained on a Varian Cary 50 scan spectrophotometer by using a rectangular quartz micro cell (Hellma, 104-QS, light path: 10 mm, 1.0 mL). Fluorescence spectroscopic studies (emission/excitation spectra) were performed with a Jasco FP-8100 spectrophotometer with a fluorescence quartz ultra-micro cell (Hellma, 105.250-QS, light path: 10 × 2 mm, 50 μL). Emission spectra were recorded under the same conditions after excitation at the corresponding wavelength (see Supporting Information Figure S3 and Table S1, excitation and emission filters: auto, excitation and emission slit = 5 nm) in DMSO. Relative quantum yields were measured in DMSO at 25°C by a relative method using a suitable standard (see Supporting Information Table S1). The following equation was used to determine the relative fluorescence quantum yield:

$$\Phi_F(x) = (A_S/A_X)(F_X/F_S)(n_X/n_S)^2\Phi_F(s)$$

where *A* is the absorbance (in the range 0.01–0.1 A.U.), *F* is the area under the emission curve, *n* is the refractive index of the solvents (at 25°C) used in measurements, and the subscripts *s* and *x* represent standard and unknown respectively.

Nomenclature of targets and ligands

Key protein targets and ligands in this article are hyperlinked to corresponding entries in http://www.guidetopharmacology.org, the common portal for data from the IUPHAR/BPS Guide to PHARMACOLOGY (Southan *et al.*, 2016), and are permanently archived in the Concise Guide to PHARMACOLOGY 2015/16 (Alexander *et al.*, 2015).

Results

Since all synthetic melatonin receptor ligands, including fluorescent ligands, are all lipophilic (Wu *et al.*, 2007; Thireau *et al.*, 2014; Zlotos *et al.*, 2014; de la Fuente Revenga *et al.*, 2015), we set out to generate a new series of hydrophilic fluorescent melatonin receptor ligands by introducing the Cy3 cyanin fluorophore known to be hydrophilic (Licha *et al.*, 2000; Tatikolov and Costa, 2002). Melatonin derivatives bearing the Cy3 fluorophore at positions N-1, C-2 or C-5 were synthesized to determine the fluorophore position most compatible with biological function. Compound **1** was coupled at the C-2 position of the indole ring with an activated acid of Cy3. Compound **2** was isolated in 40% yield (Figure S1). In order to synthesize C-5 tagged and N-1 tagged cyanine ligands, amines **4** and **6** were reacted with activated Cy3 to provide probes **5** and **7** in 53 and 89% yield respectively (Figure 1A, Supporting Information Figure S2). To generate a fluorescent lipophilic melatonin receptor probe, compound **1** was coupled with an activated acid of the BODIPY-FL® dye. This reference probe **3** was isolated as previously described (Figure 1A) (Viault *et al.*, 2016).

The spectroscopic characterization showed that the Cy3-tagged compounds **2**, **5** and **7** have a very good brightness at low energy excitation and emission wavelengths in accordance with the fluorescent properties of the cyanine 3 family (Supporting Information Figure S3 and Table S1). Compound **3** with the BODIPY fluorophore showed also excellent fluorescent properties.

The affinity of compounds **2**, **3**, **5** and **7** for human MT_1 and MT_2 receptors was then determined in competition binding experiments with 2-[^{125}I]iodomelatonin (2-[^{125}I]-MLT) in crude membranes prepared from HEK293 cells transiently expressing either receptor. Preliminary experiment showed that C-2 and C-5 tagged Cy3 ligands **2** and **5** were unable to compete 2-[^{125}I]-MLT binding at both receptors at concentrations up to 1 μM. However, ligand **7** (henceforward named ICOA-13) had micromolar affinity for both receptors (Table 1, Supporting Information Figure S4). Ligand **3** (henceforward named ICOA-9) containing the BODIPY-FL fluorophore displays sub-micromolar affinities

Table 1

Functional characteristics of ICOA-9 and ICOA-13 in HEK293 cells expressing the melatonin receptors indicated

Receptor	Ligand	2-[^{125}I]-MLT compet. pKi	ERK act. pEC_{50} (E_{max})	cAMP inh. pEC_{50} (E_{max})	ß-ARR recrut. pEC_{50} (E_{max})
hMT_1	Melatonin	−8.61 ± 0.19	−8.46 ± 0.41 (100 ± 9)	−9.37 ± 0.22 (100 ± 5)	−9.67 ± 0.17 (100 ± 5)
	ICOA-9 **(3)**	−5.76 ± 0.16	> −6 (n.d.)	−9.18 ± 0.47 (49 ± 8)	−7.60 ± 0.48 (95 ± 7)
	ICOA-13 **(7)**	−4.97 ± 0.28	> −6 (n.d.)	−7.76 ± 0.69 (37 ± 8)	−7.13 ± 0.05 (57 ± 5)
hMT_2	Melatonin	−9.3 ± 0.20	−9.16 ± 0.57 (100 ± 8)	−9.49 ± 0.11 (100 ± 5)	−9.53 ± 0.16 (100 ± 6)
	ICOA-9 **(3)**	−7.41 ± 0.05	−6.65 ± 0.21 (156 ± 23)	n.d. (n .d.)	−7.91 ± 0.72 (79 ± 8)
	ICOA-13 **(7)**	−5.48 ± 0.50	−6.58 ± 0.38 (133 ± 14)	n.d. (n.d.)	−7.76 ± 0.49 (49 ± 8)
mMT_1	Melatonin	−9.42 ± 0.28	−9.22 ± 0.86 (100 ± 14)	−9.65 ± 0.45 (100 ± 12)	n.d.
	ICOA-9 **(3)**	−6.88 ± 0.29	−6.90 ± 0.12 (146 ± 13)	−9.88 ± 0.34 (81 ± 12)	n.d.
	ICOA-13 **(7)**	−5.81 ± 0.33	−7.12 ± 0.10 (164 ± 15)	−9.60 ± 0.94 (92 ± 12)	n.d.
mMT_2	Melatonin	−9.52 ± 0.18	−8.90 ± 0.47 (100 ± 9)	−10.19 ± 0.22 (100 ± 9)	n.d.
	ICOA-9 **(3)**	−7.39 ± 0.36	−6.69 ± 0.24 (105 ± 13)	−9.60 ± 0.94 (94 ± 12)	n.d.
	ICOA-13 **(7)**	−6.24 ± 0.29	−7.24 ± 0.30 (84 ± 14)	−7.47 ± 0.65 (62 ± 8)	n.d.

Concentration–response curves were analysed by non-linear regression. Binding affinity was measured with 2-[^{125}I]-MLT and is expressed as mean pKi ± SEM (M). Agonist potency is expressed as pEC_{50} ± SEM (M). While the maximal efficacy, E_{max}, is expressed as a percentage of the maximal effect observed with melatonin (=100%). Data are mean of at least three independent experiments, each of them performed using at least eight different ligand concentrations. n.d., not determined.

for both melatonin receptors (Table 1, Supporting Information Figure S4A, B). Similar affinities were observed for mouse MT_1 and MT_2 receptors (supporting Information-Figure S4C, D).

In accordance with the reported hydrophilic property of Cy3 (Licha *et al.*, 2000; Tatikolov and Costa, 2002), ICOA-13 containing the Cy3 fluorophore was much more hydrophilic than ICOA-9 as it did not penetrate into intact cells unless permeabilized (Figure 1B). In contrast, ICOA-9 was readily penetrating into intact and permeabilized cells (Figure 1B). Therefore, ICOA-13 showed the desired properties in terms of melatonin receptor binding and absence of cell penetration. Unfortunately, the use of ICOA-13 as a fluorescent probe to label melatonin receptors for fluorescence microscopy imaging was not successful, probably due to its low binding affinity, as no specific staining was observed in melatonin receptor-transfected cells.

We next determined the functional properties of ICOA-9 and ICOA-13 in comparison to melatonin in HEK293 cells expressing human or murine MT_1 and MT_2 receptors. We first determined time-courses of ERK1/2 phosphorylation by melatonin, ICOA-9 and ICOA-13. A peak of phosphorylation was observed at 5 min for all the compounds at a saturating

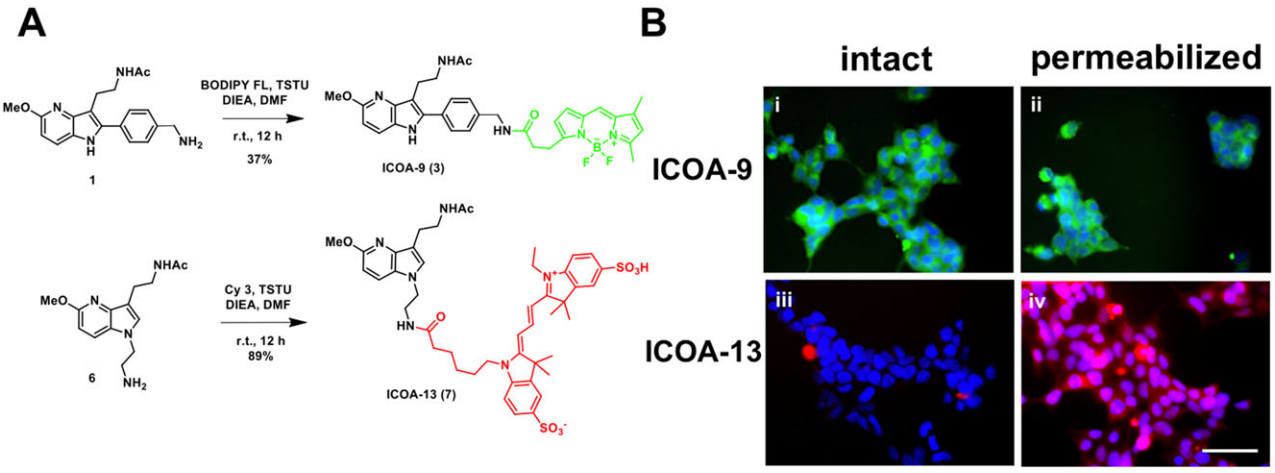

Figure 1

Chemical synthesis pathway and permeability properties of fluorescent melatonin receptor ligands. (A) Chemical synthesis of ICOA-9 (**3**) and ICOA-13 (**7**). (B) Representative fluorescence microscopy images of intact (i, iii) and permeabilized (ii, iv) non-transfected HEK293 cells incubated with 100 nM ICOA-9 (i, ii) (green) or ICOA-13 (iii, iv) (red). Cell nuclei are stained with DAPI (blue). Scale bar = 50 μm.

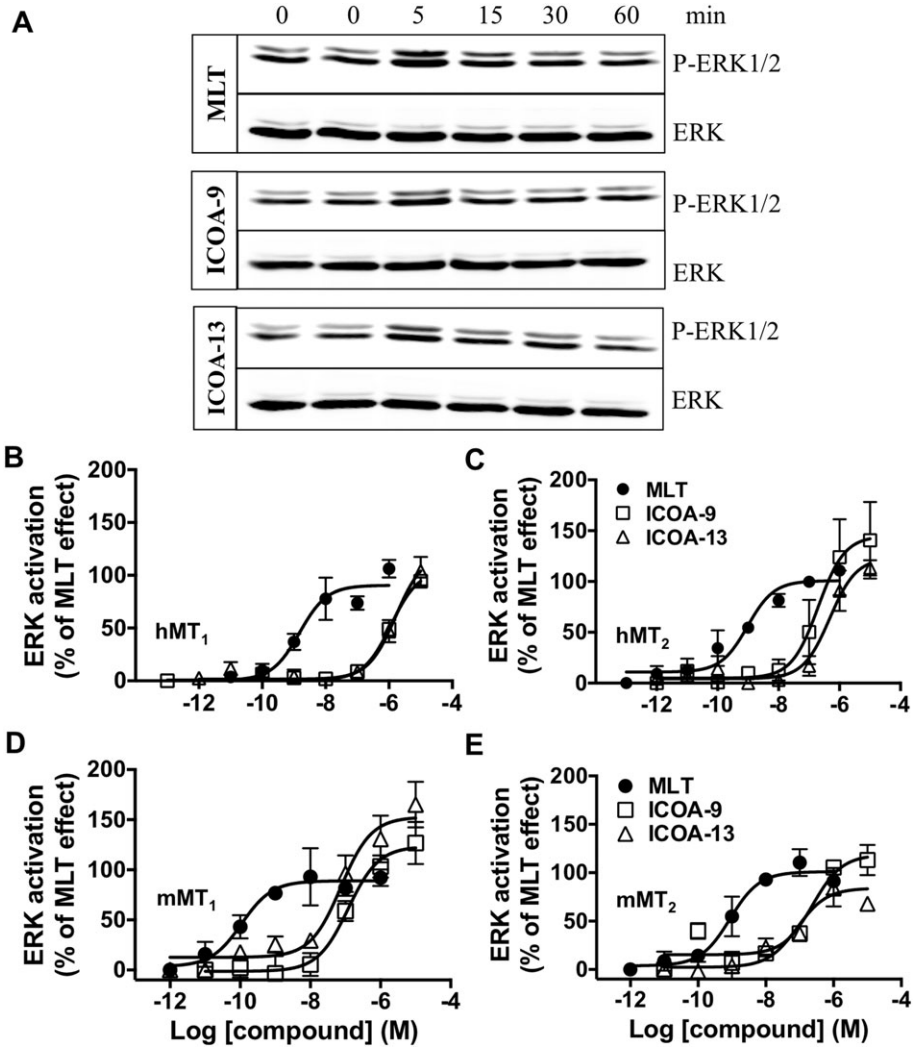

Figure 2

ERK1/2 activation triggered by melatonin, ICOA-9 and ICOA-13. Detection of phospho-ERK1/2 (P-ERK1/2) in HEK293 cells expressing hMT_1 (A, B), hMT_2 (C), mMT_1 (D) or mMT_2 (E) receptors incubated for 0 to 60 min with melatonin (100 nM), ICOA-9 (1 μM), ICOA-13 (1 μM) (Western blot; A) or at 5 min at different concentrations of the indicated ligands (Alpha-Screen assay; B, C, D, E). Data are expressed as mean ± SEM from three to four independent experiments [(B) melatonin $n = 4$, ICOA-9 and ICOA-13 $n = 3$; (C) all groups $n = 3$; (D, E) melatonin $n = 4$, ICOA-9 $n = 3$, ICOA-13 $n = 4$]. Receptor expression levels were 155 ± 62, 52 ± 22, 136 ± 63 and 112 ± 22 fmol·mg^{-1} of protein for hMT_1, hMT_2, mMT_1 and mMT_2 receptors respectively.

ligand concentration (Figure 2A). A quantitative assessment of ERK activation at 5 min was performed with the P-ERK AlphaScreen SureFire Assay that monitors P-ERK levels directly in cell lysates. ERK activation by melatonin ranged between 1.5- to 2.5-fold on human and mouse melatonin receptors, respectively, compared with the basal. ICOA-9 and ICOA-13 exhibited potencies in the sub-micromolar range except for hMT_1, for which micromolar potencies were observed (Figure 2, Table 1). The response of all ligands was abolished in the presence of pertussis toxin, indicating that activation of the ERK pathway is $G_{i/o}$ protein-dependent (Supporting Information Figure S5).

We next measured the capacity of ICOA-9 and ICOA-13 to inhibit forskolin-stimulated cAMP production. Melatonin inhibited forskolin-stimulated cAMP production at all four receptors with similar EC_{50} values in the sub-nanomolar range (Figure 3, Table 1). ICOA-9 behaved as a partial agonist (E_{max} = 49–90%), and potencies varied between receptors (pEC_{50}: between 10^{-8} M and 10^{-10} M). ICOA-13 is a full agonist for this pathway on mMT_1 receptors with potency in the sub-nanomolar range, and partial agonist for hMT_1 and mMT_2 (pEC_{50} = −7.76 ± 0.69 and −7.47 ± 0.65 respectively). For hMT_2, EC_{50} and E_{max} could not be determined as the colour of ICOA-9 and ICOA-13 interfered with the assay at concentrations higher than 1 μM respectively.

To explore another major signalling event of GPCRs, namely, the recruitment of β-arrestins, we monitored β-arrestin 2 recruitment to hMT_1 and hMT_2 receptors in response to melatonin, ICOA-9 and ICOA-13 (Figure 4A, B,

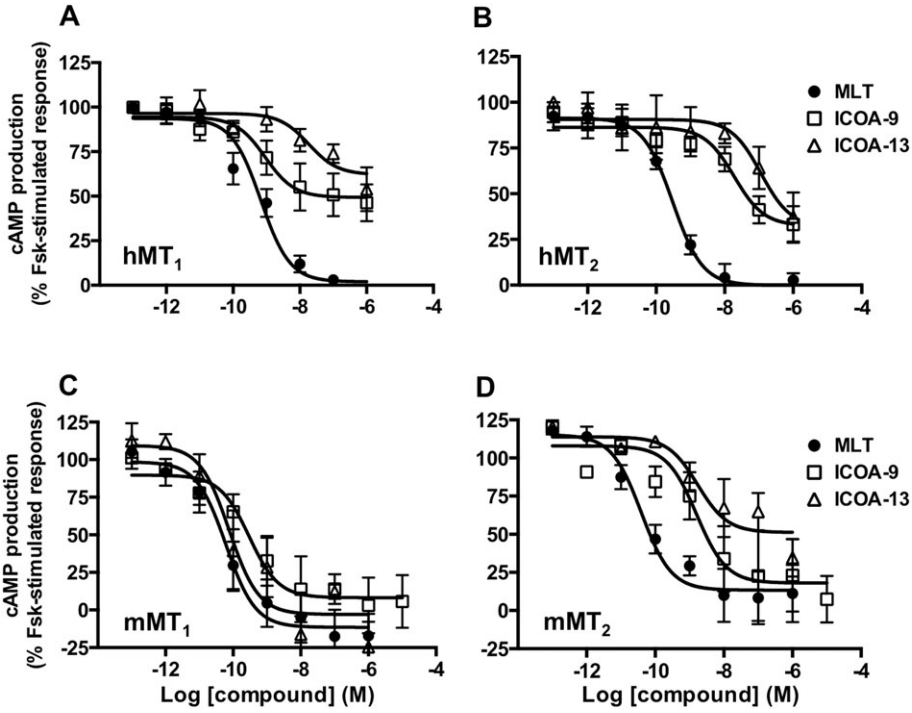

Figure 3

Inhibition of cAMP production by melatonin, ICOA-9 and ICOA-13. Inhibitory effect of melatonin, ICOA-9 and ICOA-13 on forskolin (Fsk)-stimulated cAMP production in HEK293 cells expressing hMT_1 (A), hMT_2 (B), mMT_1 (C) or mMT_2 (D) receptors. Data are expressed as mean ± SEM from 5 to 10 independent experiments [(A) melatonin $n = 10$; ICOA-9 and ICOA-13 $n = 6$; (B) melatonin $n = 7$, ICOA-9 and ICOA-13 $n = 6$; (C) all groups $n = 6$; (D) all groups $n = 5$]. Data are presented as percentage of forskolin-stimulated response and are normalized to the maximal and minimal melatonin effect. The amplitude of cAMP inhibition varied between 25 and 50%, depending on the receptor.

Table 1). We used the PathHunter assay (DiscoverX) that is based on the complementation between the PK2 tag (fused to the C-terminus of receptors) and the β-arrestin 2-β-gal-enzyme acceptor fusion protein. Addition of the PK2 tag did not modify the capacity of hMT_1 and hMT_2 to inhibit forskolin-induced cAMP production. ICOA-9 behaved as a full agonist on hMT_1 and partial agonist on hMT_2 receptors. ICOA-13 is a partial agonist for both receptors with potencies in the sub-micromolar range as ICOA-9.

Given the fact that the action of the cell-impermeable ICOA-13 is spatially restricted as compared with the lipophilic melatonin, we determined possible signalling bias of ICOA-9 and ICOA-13, by fitting dose–response curves of functional assays to the operational model of agonism designed by Kenakin and Christopoulos (Kenakin and Christopoulos, 2013) to obtain $\log(\tau/K_A)$ transduction ratios, which is a unique index of coupling efficiency (or efficacy) of an agonist. To eliminate the influence of the system and the observation biases, the activity of the compounds at a given signalling pathway was compared with that of melatonin, which served as the reference compound, and subsequently, values were expressed as $\Delta\log(\tau/K_A)$. Ligand bias for two pathways, relative to melatonin, was expressed as $10^{\Delta\Delta\log(\tau/KA)}$ as previously described (van der Westhuizen *et al.*, 2014) (Supporting Information Table S2). No bias was observed for ICOA-9 and ICOA-13 for most receptors, with the exception of hMT_1 for which ICOA-9 showed significant bias (25- and 57-fold) on the cAMP over β-arrestin and ERK pathways, respectively, when using extrapolated EC_{50} and E_{max} values for ERK activation as previously reported (Baltos *et al.*, 2016) (see Methods section) (Figure 4C, Supporting Information Table S2). Taken together, this analysis shows that the cell-permeable ICOA-9 shows bias at hMT_1 and the cell-impermeable ICOA-13 does not display any detectable signalling bias compared with the cell-permeable melatonin.

Recently, MT_1 receptors have been described to be located in brain mitochondria (Wang *et al.*, 2011). Here, we confirmed the localization of MT_1 receptors in mitochondria by its extensive colocalization with the mitochondria targeted red fluorescent protein (mito-RFP) (Figure 5A). We further measured the capacity of melatonin and ICOA-13 to inhibit forskolin-stimulated cAMP production. To this end, we used FRET-based cAMP sensors localized either in the plasma membrane (PM-ICUE) (DiPilato *et al.*, 2004) or in the outer mitochondrial membrane (OMM-ICUE) (Figure 5 B, C). Stimulation of MT_1 receptors by melatonin and ICOA-13 resulted in a comparable (40–50%) reduction of the forskolin-stimulated signal of the PM cAMP sensor (Figure 5B, C). In contrast, signals detected by the OMM cAMP sensor in the presence of melatonin and ICOA-13 were very different. Melatonin reduced the signal by 80% and ICOA-13 only by 25%. ICOA-9, similarly to melatonin, decreased the signal of the OMM cAMP sensor by 80% (Supporting Information Figure S6). These data show that

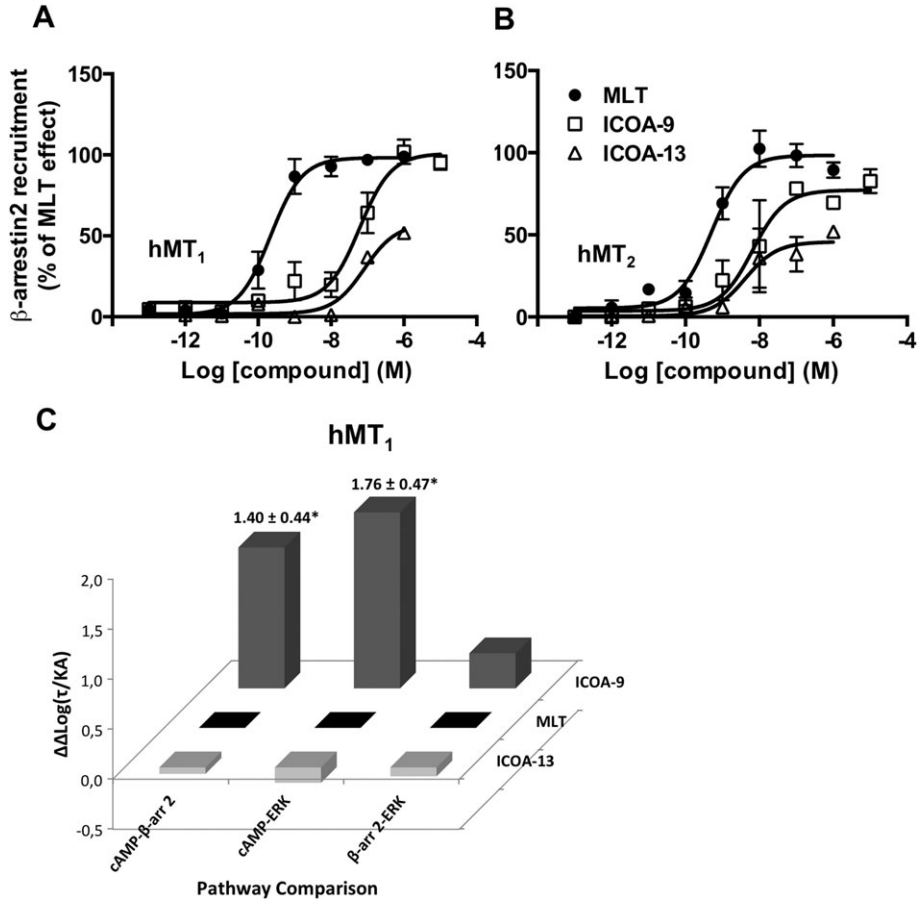

Figure 4

Recruitment of ß-arrestin2 by melatonin, ICOA-9 and ICOA-13 and signalling bias of ICOA-9. Recruitment of ß-arrestin2 to hMT_1 (A) or hMT_2 (B) receptors induced by melatonin, ICOA-9 and ICOA-13 in HEK293 cells. Data are expressed as mean ± SEM from three to four independent experiments [(A) melatonin and ICOA-9 $n = 4$; ICOA-13 $n = 3$; (B) melatonin $n = 4$, ICOA-9 and ICOA-13 $n = 3$] and are presented as percentage of melatonin effect. (C) Signalling bias factor of ICOA-9 and ICOA-13 for hMT_1 receptors presented as $\Delta\Delta\text{Log}(t/K_A)$ ratios, calculated from each individual experiment on hMT_1 receptor signalling shown in Figures 2B, 3A and 4A. *$P < 0.05$.

the cell-permeable melatonin readily decreases cAMP concentrations at the OMM, whereas cell-impermeable ICOA-13 has only a limited capacity to do so. These data validate the usefulness of the ICOA-13 compound to discriminate between plasma membrane and intracellular receptors and are consistent with the idea of mitochondrial MT_1 receptors.

Discussion

We describe here the synthesis and functional characterization of the first melatonin receptor cell-impermeant agonist that activates receptors exclusively at the cell surface. Despite the generation of numerous melatonin receptor ligands with various chemical scaffolds, all of them are lipophilic and cell permeant (Zlotos *et al.*, 2014). Introduction of a Cy3 cyanin fluorophore allowed us to significantly increase the hydrophilicity of the compound and to introduce a fluorescent label. Due to the small size of melatonin, introduction of fluorophores is technically challenging and often results in loss of binding affinity, as observed in our study for compounds **2** and **5**. ICOA-13 and ICOA-9 showed micromolar and sub-micromolar affinities, respectively, for both melatonin receptors, which were compatible with functional studies on ERK phosphorylation, cAMP inhibition and ß-arrestin2 recruitment. For fluorescence microscopy studies, ICOA-13 was inappropriate, as no specific cell surface labelling was observed in cells expressing melatonin receptors.

Emerging evidence shows that GPCR signalling can be prolonged and/or initiated in intracellular compartments such as endosomes following receptor endocytosis (Vilardaga *et al.*, 2014; Tsvetanova *et al.*, 2015). Other studies reported the presence of GPCRs in neuronal mitochondria as shown in the case of the type-1 cannabinoid receptor (Benard *et al.*, 2012; Ma *et al.*, 2015). The lipophilic nature of most cannabinoids implies that receptor–ligand interactions might occur not only at plasma membranes but also inside cells. Mitochondrial localization has been also suggested for P2Y-like, angiotensin II and 5-HT_4 receptors (Belous *et al.*, 2004; Abadir *et al.*, 2011; Wang *et al.*, 2016). In addition,

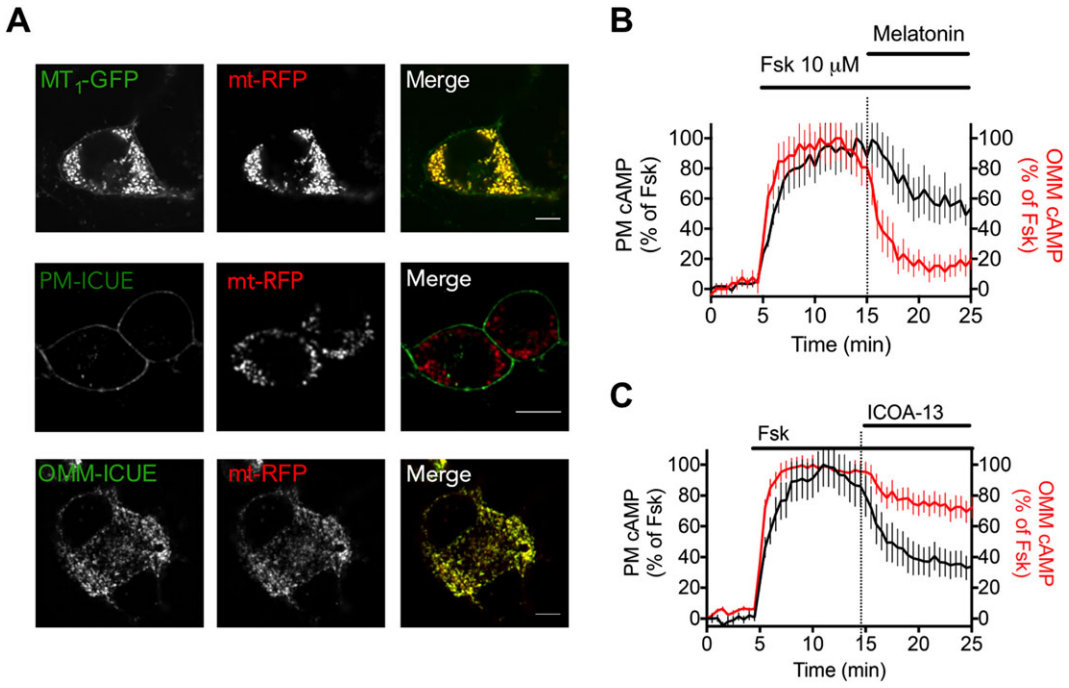

Figure 5

Mitochondrial MT_1 receptor signalling and localization. (A) Confocal imaging of N2a cells expressing MT_1-GFP or the FRET-based cAMP sensors that localized either at the plasma membrane (PM-ICUE) or the outer mitochondrial membrane (OMM-ICUE) (green) together with the mitochondrial marker mt-RFP (red). Scale bar, 10 µm. (B, C) Averaged time courses of forskolin-mediated (10 µM) cAMP production in N2a cells expressing MT_1 receptors and the FRET-based cAMP biosensors localized either at the plasma membrane (PM) or the outer mitochondrial membrane (OMM) and challenged by melatonin (100 nM) (B) and ICOA-13 (1 uM) (C). Data are expressed as the mean value ± SD, from n = 19 (MT, PM), n = 34 (MT, OMM), n = 24 (ICOA13, PM) and n = 41 (ICOA13, OMM).

several components of the cAMP pathway such as Gα and Gβ subunits of heterotrimeric G proteins and PKA, among others, have been identified in mitochondria by proteomic approaches (Chen *et al.*, 2013).

These examples indicate a new emerging paradigm of intracellular GPCR signalling in mitochondria. Melatonin receptors and its cell-penetrating ligand (melatonin) are excellent candidates for such a scenario. Indeed, melatonin has well-established protective effects on mitochondrial energy metabolism and on limiting oxidative stress (Pacini and Borziani, 2016), but the underlying molecular mechanisms are unknown. A recent study suggests that the MT_1 receptor is located in brain mitochondria (Wang *et al.*, 2011). Our data on transfected N2a cells are consistent with this finding. More rapid progress on the subcellular localization of melatonin signalling is hampered by the low expression levels of these receptors and poor quality of available tools like anti-receptor antibodies and selective ligands. The development of the ICOA-13 agonist represents a major progress in this respect. The comparison of this cell-impermeant fluorescent ligand ICOA-13 and its permeant homologue ICOA-9 showed no difference in affinity but more in efficacy and potency between human and mouse melatonin receptors. Indeed, on the cAMP pathway, ICOA-9 is more potent but partial on hMT_1 compared with mMT_1 receptors. In contrast, ICOA-13 has a better potency and is a full agonist on mMT_1 receptor versus hMT_1 receptor.

We also quantified the degree of signalling bias of each of the compounds using the operational model of agonism to determine the potential impact of the spatial restriction of ICOA-13 to the plasma membrane to signalling bias as compared with the cell-permeable ICOA-9 and melatonin. In our study, the quantification of biased agonism was calculated at a single time point for each signalling pathway which corresponds to the maximum activation of that pathway, or when the signal reaches a steady state. Different experimental conditions such as different kinetics contexts can influence the bias factor, as reported recently for a series of agonists for the dopamine D_2 receptor (Klein Herenbrink *et al.*, 2016). Despite these obvious limitations, we were able to conclude that the spatial restriction of ICOA-13 did not introduce any detectable bias compared with ICOA-9 and melatonin since all three ligands were tested in parallel using the same time points for each signalling pathway. Significant bias was observed for ICOA-9 on hMT_1 receptors with preferences for the G_i/cAMP pathway over the ß-arrestin2 and ERK pathways.

Melatonin has pleiotropic effects ranging from antioxidant and neuroprotective effects to the regulation of glucose homeostasis, circadian rhythms, sleep and retinal physiology (Dubocovich *et al.*, 2010; Tosini *et al.*, 2014). How melatonin exerts these effects remains in many cases elusive. Dysregulation of the melatonin system is associated with autoimmune disorders such as multiple sclerosis and neurodegenerative diseases such as Parkinson,

Alzheimer and also Huntington disease for which mitochondrial MT_1 receptors have been suggested to play an important role (Wang *et al.*, 2011). Cell-impermeant ligands like ICOA-13 will be precious tools to determine the contribution of mitochondrial versus plasma membrane receptors and the signalling pathways involved. This information will be essential for the design of new drugs and therapeutic strategies for melatonin-associated diseases including a controlled enhancement of melatonin's antioxidant-related effects.

Acknowledgements

This work was supported by the Agence Nationale de la Recherche (ANR 2011-BSV1-012-01 "MLT2D" and ANR-2011-META "MELA-BETES", ANR-12-RPIB-0016 "MED-HET-REC-2"), the Fondation pour la Recherche Médicale (Equipe FRM DEQ20130326503, to R.J.), Institut National de la Santé et de la Recherche Médicale (INSERM), Centre National de la Recherche Scientifique (CNRS) and the Who am I? laboratory of excellence No.ANR-11-LABX-0071 funded by the French Government through its "Investments for the Future" programme operated by The French National Research Agency (ANR) under grant No. ANR-11-IDEX-0005-01 (to R.J.); La Région Centre (APR2009-LOIREMEL to G.G. and APR2012-LIFERMEL to F. S.), Labex SynOrg (ANR-11-LABX-0029 to F.S.), the National Institutes of Health (NIH) under Award numbers R01 DK087688 (J.P.V.) and R01 DK102495 (J.P.V.) and the Cotswold Foundation Fellowship Award (F.J.A.).

Author contributions

E.C. and F.G. performed functional assays. R.G. and R.J. performed radioligand binding assays. G.V. performed synthesis and characterization of compounds **2**, **3**, **5** and **7**. F.J.A. performed experiments in N2a cells. A.K. performed analysis of biased signalling. G.G. elaborated the synthesis pathway. P.D. and R.M.F. participated in the study design. J. P.V. supervised studies in N2a cells. F.S. designed the fluorescent melatonin ligands and supervised the chemical synthesis. E.C. and R.J. wrote the article. F.G., E.C., A.L., F.S. and J.P.V. participated in the reviewing and editing of the article. R.J. elaborated and supervised the project.

Conflict of interest

The authors declare no conflicts of interest.

Declaration of transparency and scientific rigour

This Declaration acknowledges that this paper adheres to the principles for transparent reporting and scientific rigour of preclinical research recommended by funding agencies, publishers and other organisations engaged with supporting research.

References

Abadir PM, Foster DB, Crow M, Cooke CA, Rucker JJ, Jain A *et al.* (2011). Identification and characterization of a functional mitochondrial angiotensin system. Proc Natl Acad Sci U S A 108: 14849–14854.

Alexander SP, Davenport AP, Kelly E, Marrion N, Peters JA, Benson HE *et al.* (2015). The Concise Guide to PHARMACOLOGY 2015/16: G protein-coupled receptors. Br J Pharmacol 172: 5744–5869.

Ayoub MA, Levoye A, Delagrange P, Jockers R (2004). Preferential formation of MT1/MT2 melatonin receptor heterodimers with distinct ligand interaction properties compared with MT2 homodimers. Mol Pharmacol 66: 312–321.

Baba K, Benleulmi-Chaachoua A, Journe AS, Kamal M, Guillaume JL, Dussaud S *et al.* (2013). Heteromeric MT1/MT2 melatonin receptors modulate photoreceptor function. Sci Signal 6: ra89.

Baltos JA, Paoletta S, Nguyen AT, Gregory KJ, Tosh DK, Christopoulos A *et al.* (2016). Structure-activity analysis of biased agonism at the human adenosine A3 receptor. Mol Pharmacol 90: 12–22.

Becker-Andre M, Wiesenberg I, Schaeren WN, Andre E, Missbach M, Saurat JH *et al.* (1994). Pineal gland hormone melatonin binds and activates an orphan of the nuclear receptor superfamily. J Biol Chem 269: 28531–28534.

Belous A, Wakata A, Knox CD, Nicoud IB, Pierce J, Anderson CD *et al.* (2004). Mitochondrial P2Y-like receptors link cytosolic adenosine nucleotides to mitochondrial calcium uptake. J Cell Biochem 92: 1062–1073.

Benard G, Massa F, Puente N, Lourenco J, Bellocchio L, Soria-Gomez E *et al.* (2012). Mitochondrial CB(1) receptors regulate neuronal energy metabolism. Nat Neurosci 15: 558–564.

Cecon E, Chen M, Marcola M, Fernandes PA, Jockers R, Markus RP (2015). Amyloid beta peptide directly impairs pineal gland melatonin synthesis and melatonin receptor signaling through the ERK pathway. FASEB J 29: 2566–2582.

Chen X, Cui Z, Wei S, Hou J, Xie Z, Peng X *et al.* (2013). Chronic high glucose induced INS-1beta cell mitochondrial dysfunction: a comparative mitochondrial proteome with SILAC. Proteomics 13: 3030–3039.

Curtis MJ, Bond RA, Spina D, Ahluwalia A, Alexander SP, Giembycz MA *et al.* (2015). Experimental design and analysis and their reporting: new guidance for publication in BJP. Br J Pharmacol 172: 3461–3471.

de la Fuente Revenga M, Herrera-Arozamena C, Fernandez-Saez N, Barco G, Garcia-Orue I, Sugden D *et al.* (2015). New coumarin-based fluorescent melatonin ligands. Design, synthesis and pharmacological characterization. Eur J Med Chem 103: 370–373.

DiPilato LM, Cheng X, Zhang J (2004). Fluorescent indicators of cAMP and Epac activation reveal differential dynamics of cAMP signaling within discrete subcellular compartments. Proc Natl Acad Sci U S A 101: 16513–16518.

Dubocovich ML, Delagrange P, Krause DN, Sugden D, Cardinali DP, Olcese J (2010). International union of basic and clinical pharmacology. LXXV. Nomenclature, classification, and pharmacology of G protein-coupled melatonin receptors. Pharmacol Rev 62: 343–380.

Feinstein TN, Yui N, Webber MJ, Wehbi VL, Stevenson HP, King JD Jr *et al.* (2013). Noncanonical control of vasopressin receptor type 2 signaling by retromer and arrestin. J Biol Chem 288: 27849–27860.

Ferrandon S, Feinstein TN, Castro M, Wang B, Bouley R, Potts JT *et al.* (2009). Sustained cyclic AMP production by parathyroid hormone receptor endocytosis. Nat Chem Biol 5: 734–742.

Guillaume JL, Daulat AM, Maurice P, Levoye A, Migaud M, Brydon L *et al.* (2008). The PDZ protein mupp1 promotes Gi coupling and signaling of the Mt1 melatonin receptor. J Biol Chem 283: 16762–16771.

Irannejad R, Tsvetanova NG, Lobingier BT, von Zastrow M (2015). Effects of endocytosis on receptor-mediated signaling. Curr Opin Cell Biol 35: 137–143.

Jetten AM (2009). Retinoid-related orphan receptors (RORs): critical roles in development, immunity, circadian rhythm, and cellular metabolism. Nucl Recept Signal 7: e003.

Jockers R, Delagrange P, Dubocovich ML, Markus RP, Renault N, Tosini G *et al.* (2016). Update on melatonin receptors. IUPHAR Review. Br J Pharmacol 173: 2702–2725.

Jockers R, Maurice P, Boutin JA, Delagrange P (2008). Melatonin receptors, heterodimerization, signal transduction and binding sites: what's new? Br J Pharmacol 154: 1182–1195.

Kalliolia E, Silajdzic E, Nambron R, Hill NR, Doshi A, Frost C *et al.* (2014). Plasma melatonin is reduced in Huntington's disease. Mov Disord 29: 1511–1515.

Kamal M, Gbahou F, Guillaume JL, Daulat AM, Benleulmi-Chaachoua A, Luka M *et al.* (2015). Convergence of melatonin and serotonin (5-HT) signaling at MT2/5-HT2C receptor heteromers. J Biol Chem 290: 11537–11546.

Kenakin T, Christopoulos A (2013). Signalling bias in new drug discovery: detection, quantification and therapeutic impact. Nat Rev Drug Discov 12: 205–216.

Kenakin T, Watson C, Muniz-Medina V, Christopoulos A, Novick S (2012). A simple method for quantifying functional selectivity and agonist bias. ACS Chem Nerosci 3: 193–203.

Klein Herenbrink C, Sykes DA, Donthamsetti P, Canals M, Coudrat T, Shonberg J *et al.* (2016). The role of kinetic context in apparent biased agonism at GPCRs. Nat Commun 7: 10842.

Licha K, Riefke B, Ntziachristos V, Becker A, Chance B, Semmler W (2000). Hydrophilic cyanine dyes as contrast agents for near-infrared tumor imaging: synthesis, photophysical properties and spectroscopic in vivo characterization. Photochem Photobiol 72: 392–398.

Liu RY, Zhou JN, van Heerikhuize J, Hofman MA, Swaab DF (1999). Decreased melatonin levels in postmortem cerebrospinal fluid in relation to aging, Alzheimer's disease, and apolipoprotein E-epsilon4/4 genotype. J Clin Endocrinol Metab 84: 323–327.

Ma L, Jia J, Niu W, Jiang T, Zhai Q, Yang L *et al.* (2015). Mitochondrial CB1 receptor is involved in ACEA-induced protective effects on neurons and mitochondrial functions. Sci Rep 5: 12440.

Mujumdar RB, Ernst LA, Mujumdar SR, Lewis CJ, Waggoner AS (1993). Cyanine dye labeling reagents: sulfoindocyanine succinimidyl esters. Bioconjug Chem 4: 105–111.

Pacini N, Borziani F (2016). Oncostatic-cytoprotective effect of melatonin and other bioactive molecules: a common target in mitochondrial respiration. Int J Mol Sci 17.

Petit L, Lacroix I, deCoppet P, Strosberg AD, Jockers R (1999). Differential signaling of human Mel1a and Mel1b melatonin receptors through the cyclic guanosine 3 ′-5′-monophosphate pathway. Biochem Pharmacol 58: 633–639.

Reiter RJ, Tan DX, Kim SJ, Cruz MH (2014). Delivery of pineal melatonin to the brain and SCN: role of canaliculi, cerebrospinal fluid, tanycytes and Virchow-Robin perivascular spaces. Brain Struct Funct 219: 1873–1887.

Southan C, Sharman JL, Benson HE, Faccenda E, Pawson AJ, Alexander SP *et al.* (2016). The IUPHAR/BPS Guide to PHARMACOLOGY in 2016: towards curated quantitative interactions between 1300 protein targets and 6000 ligands. Nucleic Acids Res 44: D1054–D1068.

Tan DX, Manchester LC, Qin L, Reiter RJ (2016). Melatonin: a mitochondrial targeting molecule involving mitochondrial protection and dynamics. Int J Mol Sci 17.

Tatikolov AS, Costa SM (2002). Photophysics and photochemistry of hydrophilic cyanine dyes in normal and reverse micelles. Photochem Photobiol Sci 1: 211–218.

Thireau J, Marteaux J, Delagrange P, Lefoulon F, Dufourny L, Guillaumet G *et al.* (2014). Original design of fluorescent ligands by fusing BODIPY and melatonin neurohormone. ACS Med Chem Lett 5: 158–161.

Tosini G, Owino S, Guillaume JL, Jockers R (2014). Understanding melatonin receptor pharmacology: latest insights from mouse models, and their relevance to human disease. Bioessays 36: 778–787.

Tsvetanova NG, Irannejad R, von Zastrow M (2015). G protein-coupled receptor (GPCR) signaling via heterotrimeric G proteins from endosomes. J Biol Chem 290: 6689–6696.

van der Westhuizen ET, Breton B, Christopoulos A, Bouvier M (2014). Quantification of ligand bias for clinically relevant beta2-adrenergic receptor ligands: implications for drug taxonomy. Mol Pharmacol 85: 492–509.

Venegas C, Garcia JA, Escames G, Ortiz F, Lopez A, Doerrier C *et al.* (2012). Extrapineal melatonin: analysis of its subcellular distribution and daily fluctuations. J Pineal Res 52: 217–227.

Viault G, Poupart S, Mourlevat-Le Magrex S, Lagaraine C, Devavry S *et al.* (2016). Design, synthesis and biological evaluation of fluorescent ligands for MT1 and/or MT2 melatonin receptors. RSC Adv 6: 62508–62521.

Vilardaga JP, Jean-Alphonse FG, Gardella TJ (2014). Endosomal generation of cAMP in GPCR signaling. Nat Chem Biol 10: 700–706.

Wang Q, Zhang H, Xu H, Guo D, Shi H, Li Y *et al.* (2016). 5-HTR3 and 5-HTR4 located on the mitochondrial membrane and functionally regulated mitochondrial functions. Sci Rep 6: 37336.

Wang X, Sirianni A, Pei Z, Cormier K, Smith K, Jiang J *et al.* (2011). The melatonin MT1 receptor axis modulates mutant Huntingtin-mediated toxicity. J Neurosci 31: 14496–14507.

Wu PW, Cheng YM, Hsieh WT, Wang YH, Wei CY, Chou PT (2007). 7-azamelatonin: efficient synthetic routes, excited-state double proton transfer properties and biomedical implications. ChemMedChem 2: 1071–1075.

Zhang Y, Cook A, Kim J, Baranov SV, Jiang J, Smith K *et al.* (2013). Melatonin inhibits the caspase-1/cytochrome c/caspase-3 cell death pathway, inhibits MT1 receptor loss and delays disease progression in a mouse model of amyotrophic lateral sclerosis. Neurobiol Dis 55: 26–35.

Zlotos DP, Jockers R, Cecon E, Rivara S, Witt-Enderby PA (2014). MT1 and MT2 melatonin receptors: ligands, models, oligomers, and therapeutic potential. J Med Chem 57: 3161–3185.

Supporting Information

Additional Supporting Information may be found online in the supporting information tab for this article.

https://doi.org/10.1111/bph.13856

Figure S1 Synthesis of probe 2 "C2 tagging".
Figure S2 Synthesis of probes 5 "C5 tagging".
Figure S3 Absorption (Abs) and emission (Em) spectra of compounds 2, 3, 5 and 7 recorded in DMSO at 25°C.
Figure S4 Competition of 2-[^{125}I]-MLT binding by melatonin (MLT), ICOA-9 and ICOA-13. Crude membranes of HEK293 cells expressing hMT_1 (A), hMT_2 (B), mMT_1 (C) or mMT_2 (D) receptors were incubated with 0.1 nM 2-[^{125}I]-MLT and increasing concentrations of the indicated compounds. Data are expressed as mean ± S.E.M. from 3–8 independent experiments (A. melatonin n = 4, ICOA-9 n = 4, ICOA-13 n = 3; B. all groups n = 4; C. melatonin n = 8, ICOA-9 n = 7, ICOA-13 n = 6; D. melatonin n = 8, ICOA-9 and ICOA-13 n = 7). Data are represented as percentage of maximal binding in the absence of compounds and normalized to melatonin maximum effect.
Figure S5 ERK1/2 activation in the absence or presence of PTX. Detection of phospho-ERK1/2 in HEK293 cells expressing hMT_1 (A), hMT_2 (B), mMT_1 (C) or mMT_2 (D) receptors incubated for 5 min with MLT (100 nM), ICOA-9 (1 μM), ICOA-13 (1 μM) in the absence or presence of PTX (10 ng/μL, overnight). Data are expressed as mean ± S.E.M. from 5 independent experiments. *P < 0.05 compared to respective control by Student t-test, one-tail analysis.
Figure S6 Effect of ICOA-9 on cAMP production in neuroblastoma cells. Averaged time courses of forskolin-mediated (10 μM) cAMP production in N2a cells expressing MT_1 and the FRET-based cAMP biosensors localized at the outer mitochondrial membrane (OMM) and challenged by ICOA-9 (1 μM). Data expressed as the mean value ± s.d. from n = 48.
Figure S7 ^{1}H and ^{13}C NMR spectra of compound 2.
Figure S8 ^{1}H and ^{13}C NMR spectra of compound 5.
Figure S9 ^{1}H and ^{13}C NMR spectra of compound 7 (ICOA-13).
Table S1 Photophysical and physicochemical properties of compounds 2, 3, 5 and 7.
Table S2 $\Delta\Delta\log(\tau/K_A)$ ratios and bias factors for ICOA-9 and ICOA-13 at the hMT_1, hMT_2, mMT_1 and mMT_2.